Title

Effects of sawtooth heat pulses on edge flows and turbulence in a tokamak plasma

Journal

Plasma Science and Technology, 25(1)

ISSN

1009-0630

Authors

Kaijun, ZHAO

NAGASHIMA, Yoshihiko

Zhibin, GUO

et al.

Publication Date

2022

DOI

10.1088/2058-6272/ac7c60

Peer reviewed

Authors' final version
Published as: *Plasma Sci. Tech.* **25**, 015101, 2023
https://doi.org/10.1088/2058-6272/ac7c60

Effects of sawtooth heat pulses on edge flows and turbulence in a tokamak plasma

Kaijun ZHAO (赵开君)[1,*], Yoshihiko NAGASHIMA[2], Zhibin GUO (郭志彬)[3], Patrick H DIAMOND[4,5], Jiaqi DONG (董家齐)[5], Longwen YAN (严龙文)[5], Kimitaka ITOH[6,7,8], Sanae-I ITOH [2,7, 9,†], Xiaobo LI (李晓博)[3], Jiquan LI (李继全)[5], Akihide FUJISAWA[2], Shigeru INAGAKI[2], Jun CHENG (程钧)[5], Jianqiang XU (许健强)[5], Yusuke KOSUGA[2], Makoto SASAKI[2], Zhengxiong WANG (王正汹)[10], Huaiqiang ZHANG (张怀强)[1], Yuqian CHEN (陈俞钱)[1], Xiaogang Cao (曹小岗)[1], Deliang YU (余德良)[5], Yi LIU (刘仪)[5], Xianming SONG (宋显明)[5] , Fan Xia (夏凡)[5], and Shuo WANG (王硕)[5]

[1] School of Nuclear Science and Engineer, East China University of Technology, Nanchang 330013, People's Republic of China

[2] Research Institute for Applied Mechanics, Kyushu University, Kasuga 816-8580, Japan

[3] School of Physics, Peking University, Beijing 100871, People's Republic of China

[4] Center for Momentum Transport and Flow Organization, University of California at San Diego, California 92093, USA

[5] Southwestern Institute of Physics, Chengdu 610041, People's Republic of China

[6] Institute of Science and Technology Research, Chubu University, Aichi 487-8501, Japan

[7] Research Center for Plasma Turbulence, Kyushu University, Kasuga 816-8580, Japan

[8] National Institute for Fusion Science, Toki 509-5292, Japan

[9] Department of Innovative Energy Science and Engineering, Graduate School of Engineering, Chubu University, Aichi 487-8501, Japan

[10] School of Physics and Optoelectronic Technology, Dalian University of Technology, Dalian 116024, People's Republic of China

E-mail of corresponding author: kjzhao@ecut.edu.cn

Abstract

The enhancements of the edge zonal flows, radial electric field and turbulence are observed

[†] Prof. Sanae-I Itoh is deceased.

in ECRH heated plasmas [K. J. Zhao *et al*, Nuclear Fusion 2013, 083011]. In this paper, the effects of sawtooth heat pulses on the flows and turbulence are presented. These experiments are performed using multiple Langmuir probe arrays in the edge plasmas of the HL-2A tokamak. The edge zonal flows, radial electric fields, and turbulence are all enhanced by sawteeth. The propagation of the zonal flow and turbulence intensities is also observed. The delay time of the maximal intensity of the electric fields, zonal flows, and turbulence with respect to the sawtooth crashes is estimated as ~ 1 ms and comparable to that of the sawtooth-triggered I-phases. Not only the zonal flows but also the radial electric fields lag behind the turbulence. Furthermore, the intensities of both the zonal flows and electric field nearly linearly increase/decrease with the increase/decrease of the turbulence intensity. A double source predator-prey model analysis suggests that a relatively strong turbulence source may contribute to the dominant zonal flow formation during sawtooth cycles.

Keywords: tokamak, sawtooth heat pulse, zonal flow, turbulence, limit cycle

(Some figures may appear in colour only in the online journal)

1. Introduction

Sawtooth, a nonlinear oscillation phenomenon in core plasmas of tokamaks is an active research area in the fusion field since it has been observed on ST tokamak [1]. The study of the effects of sawtooth heat pulses on the flows and turbulence aims to understand and control plasma confinement and transport. Presently, it is an urgent task to the lower power threshold to access high confinement mode (H-mode) for ITER. The confinement regime transitions can be triggered by sawtooth heat pulses experimentally [2–5]. Sawteeth may offer a way to access H-modes, if their deleterious effects can be mitigated. As the sawtooth heat pulse propagates to edge plasmas, the edge flows and turbulence will be varied significantly [6]. Some deleterious instabilities, such as neoclassical tearing modes can also be induced by large sawteeth [7, 8].

The sawtooth, sometimes called internal disruption, can lead to repetitive density pulse, heat pulse, and turbulence clump propagations from core to edge plasmas. Thus, the properties of turbulence and transport during benign disruption have attracted much more attention in the

recent years. The measurement of heat pulses due to the sawtooth instability shows that the heat diffusivity is significantly larger than that from power balance analysis [9]. The identification of the causal relationship between heat fluxes and local temperature gradients suggests that the ballistic heat transport exists during sawtooth cycles [10].

The sawtooth oscillation can change flows via changing edge density, temperature, gradient, and turbulence. It is well recognized that $E\times B$ sheared flows play important roles in confinement regime transitions in high temperature plasmas. Generally, such flows exist in the forms of zonal flows self-generated by turbulence and mean flows driven by ion pressure gradients [11–20]. Two kinds of zonal flows, i.e, low frequency zonal flows (LFZFs) [11–17] and geodesic acoustic modes (GAMs) [19–22] are found in toroidal plasmas. The increases in turbulence levels due to sawteeth were observed using Langmuir probe arrays [6, 23] and by CO_2 laser forward scattering [24]. The GAM was observed to be reduced significantly by sawteeth [6]. The fluctuation-driven particle and heat fluxes can be enhanced due to sawtooth crashes in the edge plasmas [23]. However, sawtooth effects on the LFZFs and the time delay of turbulence with respect to sawtooth crashes have not been observed experimentally.

Slowly increasing heating power near the H-mode power threshold, an intermediate, quasi-periodic state, called the I-phase, dithering H-mode, or a limit-cycle oscillation (LCO) was detected. In the I-phase, turbulence, zonal and mean flows all couple with the pressure gradient. Extensive studies of the I-phases suggest that the flow-turbulence interaction contributes to H-mode triggering [25]. The I-phase is quite distinct from the I-mode operating regime on the Alcator C-Mod tokamak that is a steady-state regime [26]. The I-phase can be triggered by sawtooth heat pulses [3].

Here, the enhancement of the edge zonal flows, radial electric field, and turbulence during sawtooth cycles is presented. The estimated delay time of the edge flows and turbulence with respect to sawtooth crashes is ~ 1 ms in low confinement mode (L-mode) plasmas and comparable to the evaluation of that of L-I transitions. Double source predator-prey model analysis suggests that the dominant zonal flows could be driven by the relatively strong turbulence burst propagation during sawtooth cycles.

The rest of this work is organized as follows. The experimental set-up is given in section 2.

The experimental results, described in section 3, include the sawtooth propagation, sawtooth modulation on turbulence and flows, conditional average analyses of the edge flows and turbulence, trajectories of turbulence and flows, analysis of a double-source predator-prey model, the radial structure of the LFZF and turbulence, and sawtooth-triggered I-phases, etc. Section 4 presents the conclusion and discussion.

2. Experiment setup

These experiments were performed in deuterium plasmas on the HL-2A tokamak with limiter and diverter configurations. The major radius of the HL-2A tokamak is R = 1.65 m and its minor radius is a = 0.4 m (limiter discharge) and 0.38 cm (diverter discharge). The limiter is at the outer midplane. First, the zonal flows, radial electric fields and turbulence relating to sawtooth crashes are measured in ECRH heated plasmas with limiter configuration. The on-axis ECRH is used and its power ~ 500 kW far below the power threshold of L-H transitions is inputted. The plasma parameters are the toroidal magnetic field B_t = 1.2–1.3 T, the plasma current I_p = 150–180 kA, the line averaged electron density N_e = 1–2×10^{19} m^{-3}, and the safety factor q_a = 3.3. Multiple Langmuir probe (LP) arrays were used to measure floating potential fluctuations, as shown in figures 1(a) and (b). A LP array of 3 tips and a four-tip LP array form a fast reciprocating probe set of 7 tips with poloidal span of 65 mm. A radial rake probe array of 12 tips is located in the poloidal cross section ~ 2100 mm away from the set of 7 tips toroidally. Next, the flows and turbulence are detected following sawtooth crashes and prior to I-phases in diverter discharge with neutral beam injection (NBI) of ~ 1 MW. The NBI power is close to, but still below, the threshold of the L-H transition. The line averaged electron density (the safety factor) is N_e = 2–3×10^{19} m^{-3} (q_{95} = 4.0). The toroidal magnetic field and plasma current are the same as those with limiter discharges. Here, the LP arrays were changed and just a fast reciprocating probe array with two steps and 12 tips was used to yield floating potential, temperature, density, Mach number [27, 28], as shown in figure 1(c). All the LP arrays were mounted on the middle plane outside of the machine. The length and diameters of all the tips are 3 mm and 2 mm, respectively [29, 30]. The sampling rate of the probe data is 1 MHz corresponding to Nyquist frequency of 500 kHz. A multiple-channel soft X-ray system is

applied to observe the sawtooth oscillations. The viewing chords are vertical and the radial positions of the chord centers can be evaluated by the EFIT code. A single channel H_α array that views crossing the core plasmas from the low to high field side at the midplane is utilized to monitor the edge region. A single channel array means that there is a photomultiplier tube. Figures 2(a) and (b) show the MHD equilibrium configurations reconstructed by the EFIT code in limited and diverted plasmas, respectively.

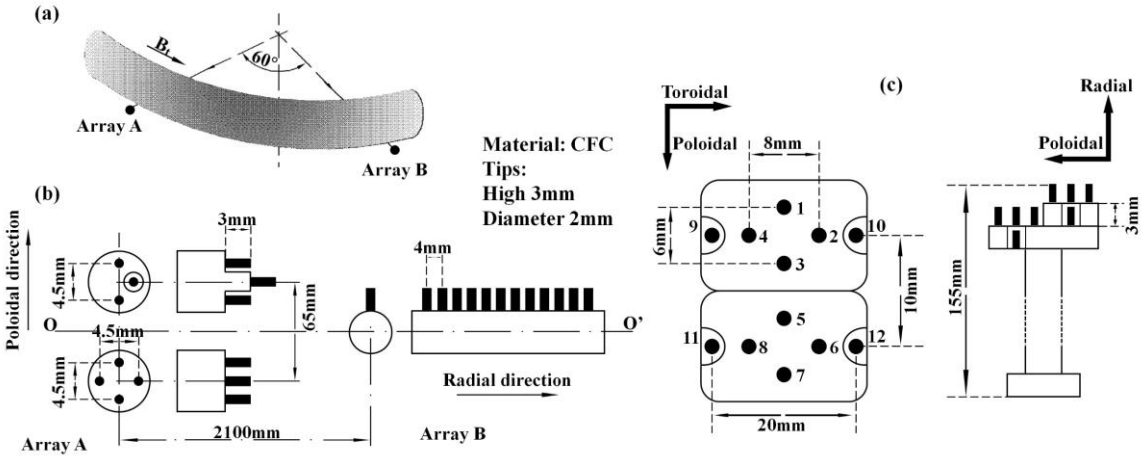

Figure 1. Layout and structure of the LP arrays: (a) plasma column, and probe arrays in limiter (b) and diverter (c) configurations.

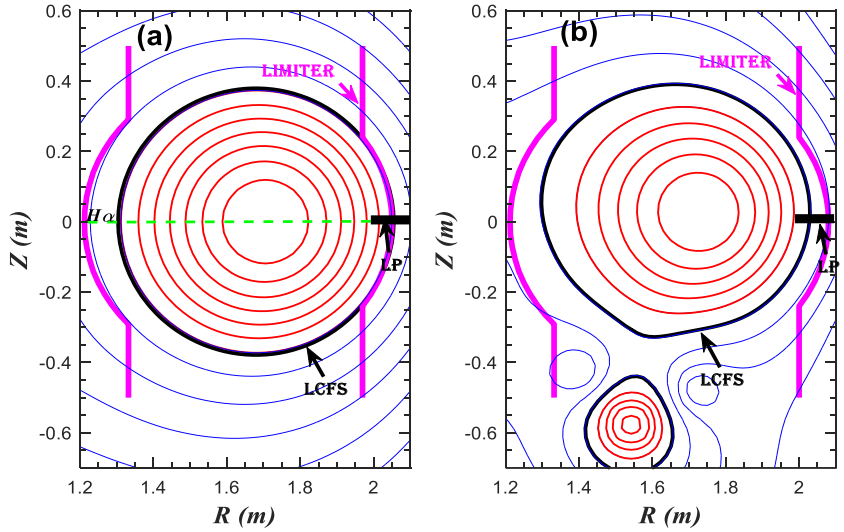

Figure 2. Equilibrium reconstructions: (a) limiter, (b) divertor.

3. Experiment results

3.1. Sawtooth propagation

The sawtooth propagation is an important feature due to its relevance to not only the core plasmas, but also the edge plasma parameters. Figures 3(a)–(d) show soft X-ray signals at various positions in the ECRH heating plasmas. The sawtooth crash starts at ~ 602.4 ms at the position of r ~ 2.5 cm and sharply drops to the minimum value. However, a rapid increase in the intensity of the soft X-ray at r ~ 16.3 cm appears and propagates to the edge after the sawtooth crash. The significant difference of the sawtooth signals at r ~ 2.5 and 16.3 cm comes from their positions, i.e., inside and outside of the q = 1 surface. The q = 1 surface is roughly evaluated as ~ 15 cm from the measurements of the soft X-ray signals. The propagation time of the sawtooth heat pulses from r ~ 16.3 cm to r ~ 26.9 cm is by about 0.9±0.1 ms and the corresponding propagation velocity is estimated as ~ 130 m s^{-1}.

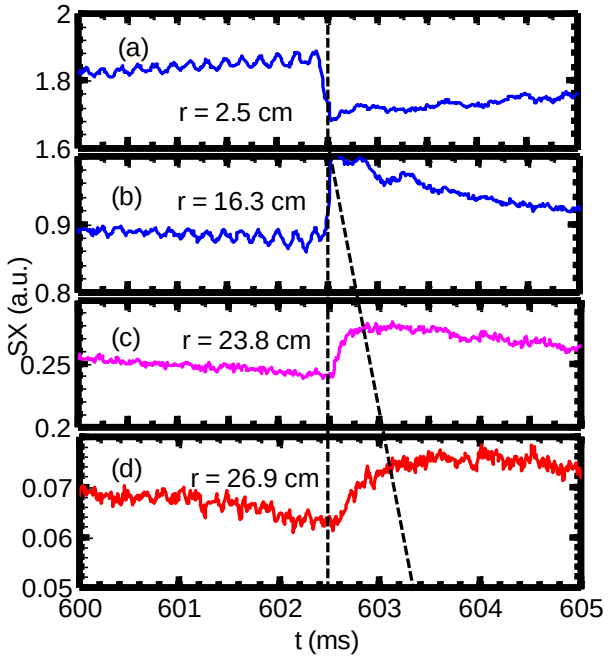

Figure 3. (a)–(d) The soft X-ray signals at various positions in ECRH heated plasmas.

Sawtooth crashes have significant effects on the temperature, density, and pressure gradient. Figure 4 shows the conditional average of the gradients of the soft X-ray signals at various positions. The conditional average is often utilized to detect the coherent mode signals. Normally, this method requires a reference signal. In this case, the sawtooth crash is considered as a reference signal and calculated by the time derivative of the soft X-ray signals. Near the

maximum of the derivative, $t_d = 0$ is defined, then the data from $t_d = -2.5$ ms (before the sawtooth crash) to 2.5 ms (after the sawtooth crash) are selected for each sawtooth crash. Here, a total of 20 sawtooth crashes are averaged. The radial distribution of the gradient of the soft X-rays is similar to that of their intensities, i.e., the gradient decreases (increases) inside (outside) of the $q = 1$ surface. The propagation time of the gradient from $r = 18.25$ cm to 28.25 cm is evaluated as ~ 0.9±0.1 ms and its velocity is calculated as ~ 130 ms^{-1}. The intensity of the soft X-rays is associated with density and temperature. Note that the soft X-ray intensity also depends on the presence of impurities although the correlation between impurities and soft X-ray intensity is beyond our discussion in this paper. This result suggests that the gradient propagates during sawtooth cycles.

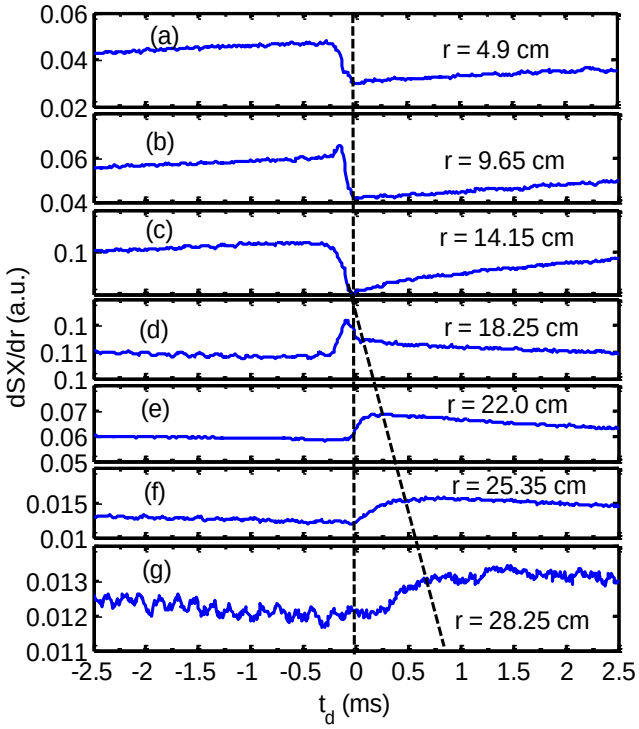

Figure 4. (a)–(g) Conditional average of gradients of soft X-ray signals at various positions in ECRH heated plasmas (the LCFS is located in $r = 40$ cm).

3.2. Sawtooth modulation on turbulence and flows

As the sawtooth heat pulse propagates to the edge plasmas, the turbulence, zonal flow and radial electric field are modulated in ECRH heated plasmas. Figures 5(a)–(d) present the soft X-ray signals at r ~ 2.5 cm, floating potentials at r ~ 37 cm, the intensity of the turbulence in

the frequency bands of 20–200 kHz and the radial electric field E_r at $r \sim 35.7$ cm, respectively. Both turbulence and radial electric field are well correlated with the sawteeth. After sawtooth crashes, the intensity of the turbulence increases and E_r drops rapidly. Considering that the change of the electron temperature is small at the radial separation of 4 mm, the E_r is roughly evaluated from the floating potentials at two radial positions, i.e $E_r = (\overline{\delta\phi_{f1}} - \overline{\delta\phi_{f2}})/d_r$, where, $\overline{\delta\phi_{fi}}$ ($i = 1, 2$) and d_r are the potential fluctuations and the radial distance, respectively.

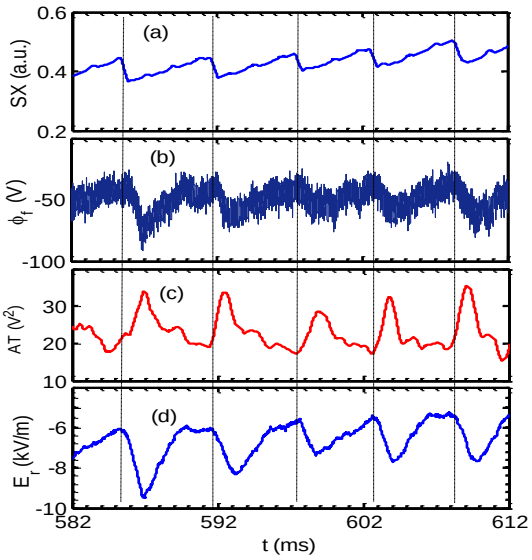

Figure 5. (a) Soft X-ray signals at $r \sim 2.5$ cm, (b) floating potential at $r \sim 37$ cm, (c) turbulence intensity and (d) radial electric field at $r \sim 35.7$ cm in ECRH heated plasmas (the LCFS is located in $r = 40$ cm).

The observation suggests that the sawteeth propagate to the edge and significantly impact the edge turbulence and flows. Usually, in the HL-2A, the width of the scrape-off layer is $\lambda_{T_e} =$ 2–6 cm for the L-mode plasmas and the pedestal width is ~ 3 cm for the H-mode plasmas.

Figure 6 shows the auto-power spectra of potentials less than 100 kHz from 582 to 612 ms at two positions of $r = 37$ and 37.4 cm. In this analysis, fast Fourier transform (FFT) is used and the component at the frequency of ~ 0.2 kHz is filtered out to remove the sawtooth oscillations in the floating potential fluctuations. A large power fraction in the frequency region of 0–3 kHz is the LFZFs. A sharp peak of ~ 10.5 kHz is identified as a mesoscale electric fluctuations (MSEFs), which has dominant GAMs and $m/n = 6/2$ components [30, 31]. The MSEF results from the nonlinear synchronization of the GAMs and magnetic fluctuations. The

m and *n* are the poloidal and toroidal mode numbers, respectively. The LFZFs and GAMs are detected by long range correlations using potential fluctuations measured simultaneously using Langmuir A and B probe arrays with a toroidal angle of 60°, as seen in figure 1(a). The $n = 0$ for both the LFZFs and GAMs are directly evaluated from the floating potentials with the toroidally distributed probe arrays. Combining potentials with Mirnov signals from magnetic coils set up in the vessel wall, the $m/n = 6/2$ component can also be identified at the MSEF frequency. Except for the tearing mode of $m/n = 6/2$, no significant oscillation in the LFZF and MSEF frequency bands is observed from the Mirnov signal. The feature at ~ 60 kHz is ambient turbulence. The ion-ion collision frequency is estimated as 2.0×10^4 s^{-1}. The radial width of the LFZFs usually is about 1–2 cm in the HL-2A and we are not sure that the sawteeth can affect this width in the present stage.

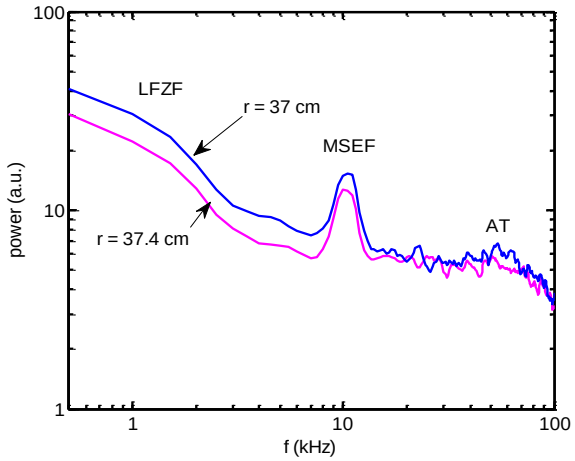

Figure 6. The auto-power spectra of the floating potential fluctuations less than 100 kHz at two radial positions in ECRH heated plasmas.

It is reasonable to imagine that turbulence-driven zonal flows are modulated by sawteeth via varying turbulence. Figures 7(a)–(b) present the soft X-ray signals at $r \sim 2.5$ cm and the spectrograms of potential fluctuations in the frequency less than 15 kHz at $r \sim 35.7$ cm, respectively. Following sawtooth crashes, the intensity of the LFZFs less than ~ 3 kHz increases while that of the MSEFs at the frequency of ~ 10.5 kHz decreases. In contrast, before sawtooth crashes, the former decreases while the latter increases. The phase between LFZFs and MSEFs during sawtooth cycles cannot be explained in the present stage. The summed powers of the

turbulence in the frequency bands of 20–200 kHz and the LFZFs are given in figures 6(c) and (d), respectively. The sawtooth modulations on the turbulence and the LFZFs are clearly shown. Note that the observation does not depend on the selection of the time window of the data.

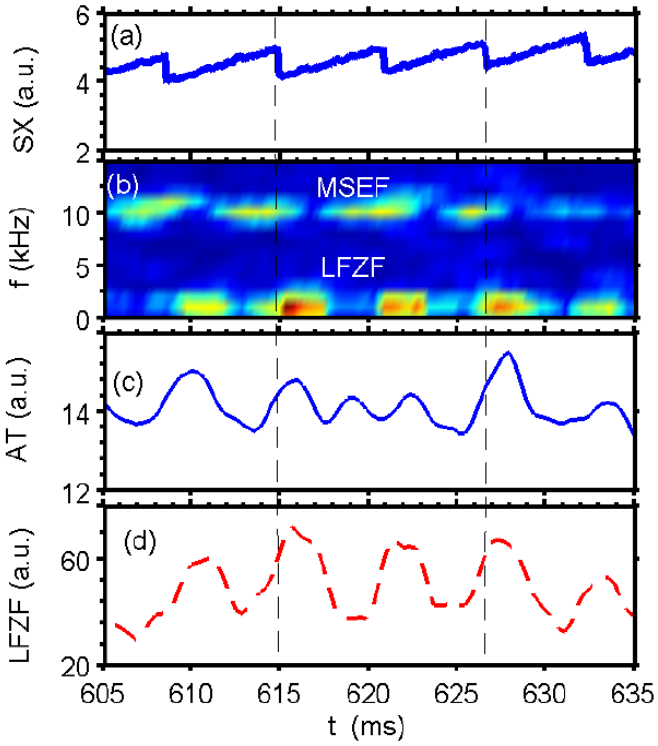

Figure 7. (a) Soft X-ray signals, (b) spectrogram of the floating potential fluctuations, (c) turbulence amplitude and (d) LFZF amplitudes in ECRH heated plasmas.

3.3. Conditional average analyses of the edge flows and turbulence

The delay time of the edge flows and turbulence with respect to sawtooth crashes in L-mode plasmas is an important parameter to understand the sawtooth propagation and confinement regime transitions. The conditional average method is utilized to estimate the delay time. Figures 8(a)–(d) show the conditional average of the soft X-ray signals at $r \sim 2.5$ cm, intensities of turbulence in the frequency band of 20–200 kHz, LFZF in the frequency bands of 0.5–3 kHz, and radial electric field E_r in ECRH heated plasmas, respectively. Before sawtooth crashes, the intensities of the turbulence, E_r, and LFZFs slowly decrease while following sawtooth crashes, they all increase rapidly. The growth time of them is roughly ~ 1.0 ms while their decay time is ~ 4.0 ms and much longer than their growth time. The LFZFs and E_r lag behind turbulence and the intensity of the LFZFs (E_r) increases faster from $t_d \sim 0.2$ to 1.2 ms

(1.0 ms). The delay times of the maxima of the LFZF, E_r, and turbulence intensities with respect to sawtooth crashes are ~ 1.2±0.2, 1.0±0.2, and 0.80±0.2 ms, respectively. The discrepancy of the delay times for the LFZF, E_r and turbulence may come from the difference in their driving mechanisms. Compared with the soft X-ray signals, it seems that turbulence intensity propagation is faster than that of the heat pulses. The delay time ~ 0.4 ms of LFZFs with respect to the turbulence is longer than the turbulence decorrelation time or energy transfer time between LFZFs and turbulence. The possible reason is that the critical value of the turbulence intensity is needed for the zonal flow driving and this will be discussed next. In addition, the intensity of the turbulence (E_r) rises up by 50% (30%). For the LFZF, its intensity is increased by 100%. This indicates that the edge turbulence, zonal flows, and E_r can be significantly enhanced by sawtooth heat pulses.

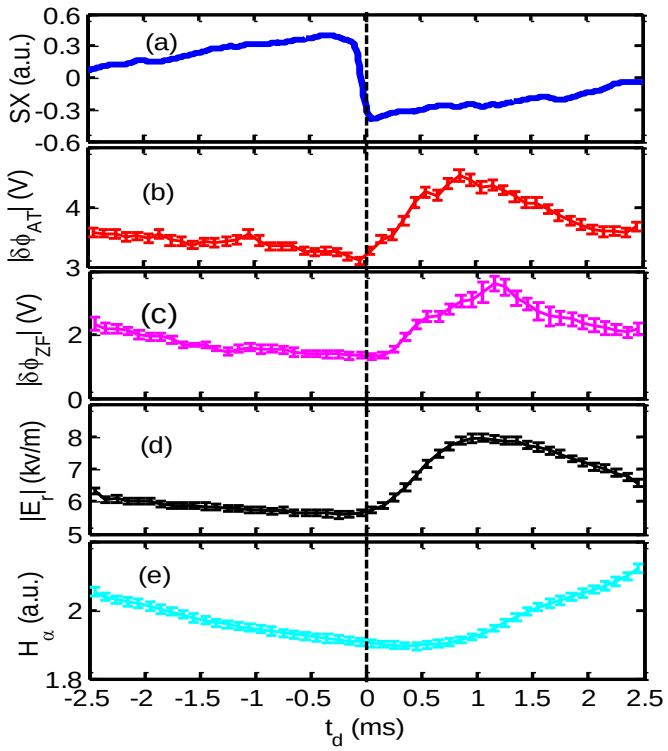

Figure 8. Conditional average of (a) soft X-ray signals, (b) turbulence intensity, (c) LFZF intensity, (d) E_r intensity and (e) H_α signals in L-mode plasmas with ECRH power ~ 500 kW.

The conditional average of H_α signals is described in figure 8(e). The H_α intensity is proportional to the plasma density in the edge region. After sawtooth crashes ~ 0.8 ms, the H_α intensity rises rapidly. The observation shows that the sawteeth can also induce density pulses

propagating to the edge. However, the delay time of H_α signals with respective to sawteeth is larger than those of the LFZFs, E_r, and turbulence. The possible reason is that their measurement points are not at the same radial position.

3.4. Trajectories of turbulence and flows, and model analysis

The role of turbulence in driving flows during sawtooth disruptions is another interesting problem for understanding the mechanism of sawtooth propagation in L-mode plasmas. Figures 9(a) and (b) give the trajectories of the intensity of the LFZF and turbulence, and of the E_r and turbulence in phase space during sawtooth cycles. Note that the E_r also contains the contribution of the zonal flows or turbulence-driven flows based on the radial force balance. Significant cycles in the trajectories are shown and rotate in the clockwise direction. The rotation direction indicates that the development of the turbulence is prior to that of the LFZFs and the E_r. This result suggests that the sawtooth-induced LFZFs and E_r may be driven dominantly by turbulence. In addition, the LFZFs and turbulence, and the E_r and turbulence are all nearly out of phase and similar results are obtained at different radial positions.

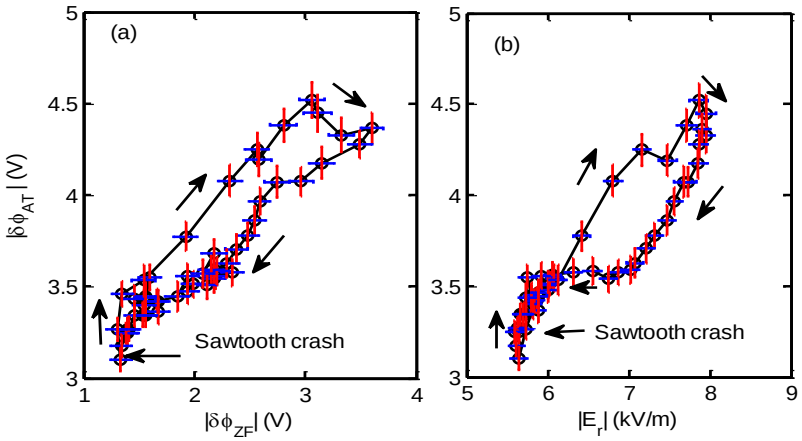

Figure 9. Trajectories of the intensities of the LFZF and turbulence (a), and of the radial electric field and turbulence (b) in phase space in ECRH heated plasmas. The arrows indicate the rotation direction of the cycles.

We also observe that the intensities of both the LFZF and the E_r nearly linearly increase/decrease with the increase/ decrease of the turbulence intensity, as shown in figure 8. This result suggests that the ratios of the LFZF power to the turbulence one and the E_r power to the turbulence one nearly keep constant.

Note that the intensity of the turbulence ramps up fast while those of the LFZF and the electric field changes little just after sawtooth crashes. This suggests that the flows might be driven less effectively when the turbulence is below the critical value.

The sawtooth heat pulses contain not only the heat pulses but also turbulence bursts. As the sawtooth heat pulse propagates to the edge, the edge pressure gradients and flows change significantly. The heat pulse and turbulence are responsible for the pressure gradient and zonal flow formations, respectively. Thus, the sawtooth effects on the flows and turbulence should link to the relative intensity of the heat pulse and turbulence burst.

In order to understand the effects of sawtooth heat pulses on the edge flows and turbulence deeply, a double-source predator-prey model is developed [31]. Similar to the 0-D model [32], four equations are utilized to describe the radial force balance and time evolutions of the ion pressure gradient P', zonal flow V_{ZF}, and turbulence intensity ε, respectively.

$$E_r = -|P'|/en - B_\phi V_{\mathrm{ZF}} \quad (1)$$

$$\partial|P'|/\partial t = -a_1\varepsilon|P'| - a_2|P'| + Q_0 + \delta Q \quad (2)$$

$$\partial V_{\mathrm{ZF}}/\partial t = b_1\varepsilon V_{\mathrm{ZF}} - b_2 V_{\mathrm{ZF}} \quad (3)$$

$$\partial\varepsilon/\partial t = \varepsilon|P'| - c_1\varepsilon^2 - c_2\varepsilon E_r'^2 + \delta S \quad (4)$$

where, $-e$, n and B_ϕ are the electron charge, density and toroidal magnetic field, respectively. The coefficients a_i, b_i and c_i are the model-dependent parameters. Considering that the sawtooth heat pulse consists of heat and turbulence pulses, the heat source δQ (turbulence source δS) from the core enters into the equation of time evolution of the pressure gradient (turbulence intensity). These equations define a nonlinear system with two external sources. For simplicity, the mean toroidal and poloidal flows are ignored. The radial electric field mainly comes from pressure gradient and zonal flows. The flows are determined by the driving and damping effects. Turbulence is from the core and enhanced by the local gradient. The heat source mainly impacts the pressure gradient.

This model is used to analyze the interaction between flows and gradient and turbulence during sawtooth cycles through varying the ratio of the δQ and δS. With lower equilibrium pressure gradient P_0', a force oscillation pattern occurs due to the sawtooth-shaped heat and turbulence sources and this is consistent with the present measurement. The shapes of the

intensities of the zonal flow $\delta\phi_{\mathrm{ZF}}$, radial electric field shear E_r' and pressure gradient P_r' are all similar to those of turbulence and heat pulses. Here, a relatively strong turbulence source is selected. The turbulence and heat source are shown in figures 10(a) and (b), respectively. The turbulence source is slightly faster than the heat source. Figures 10(c) and (d) present the trajectories of the intensities of the $\delta\phi_{\mathrm{ZF}}$ and turbulence, and of E_r' and turbulence in phase space, respectively. Two significant cycles appear and all rotate in the clockwise direction. This clearly shows that the $|\delta\phi_{\mathrm{ZF}}|$ and $|E_r'|$ follow the turbulence. The result may qualitatively explain that the turbulence-driven flow is dominant during sawtooth cycles. Compared to the experiment observation, the nearly linear intensity dependence of the LFZF and the E_r on the turbulence does not appear. Also, this simulation does not show the critical value effects of the turbulence on the flows. In addition, a 'figure-eight pattern' shown in figure 10(d) suggests that the relationship of the time sequence between the flows and turbulence changes during the sawtooth cycles. However, this is not detected in the present experiment. Note that both the $|E_r'|$ and $|E_r|$ refer to the intensity of the shear flows. A larger intensity of the E_r will cause a larger $|E_r'|$. Thus, the difference of the $|E_r|$ and $|E_r'|$, shown in figures 8(b) and 9(d), can be neglected.

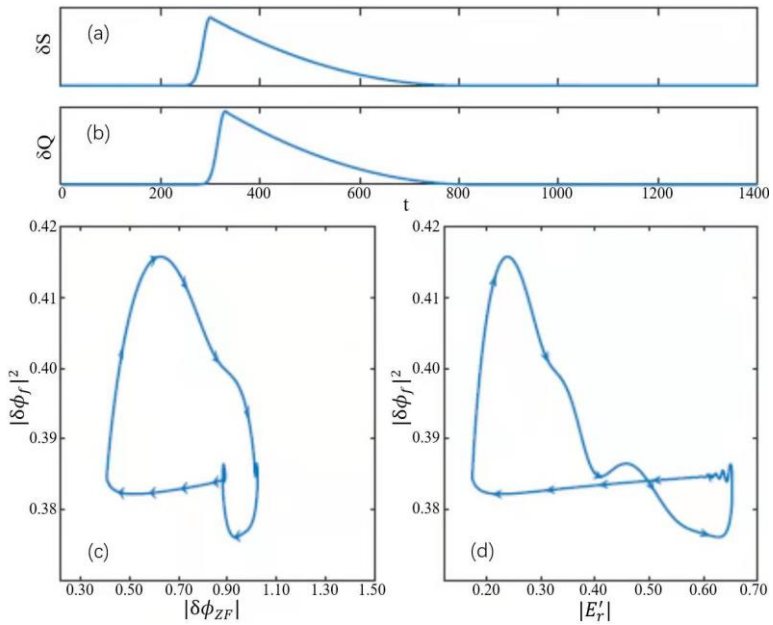

Figure 10. (a) Turbulence source, (b) heat source, and the trajectories of the intensities, (c) of the $\delta\phi_{\mathrm{ZF}}$ and turbulence, and (d) of E_r' and turbulence in phase space.

The values of various parameters used in our numerical studies are similar to those of reference [32]. We found that a scan of those parameters only leads to a small expansion or shrinkage of the stable regions of the fixed points of the equations, and does not change the conclusion, qualitatively. The qualitative performances of the trajectory, including the rotation direction and how many times it reverses, are depended on the control parameters δQ, δS and the equilibrium ion pressure gradient $|P_0'|$. Changing the systematical coefficients and under the appropriate control parameters, the system can also evolve into a forced oscillation state. The detailed discussion can be found in the reference [31].

3.5. Radial structure of the LFZF and turbulence

The radial structures and propagation of sawtooth-induced LFZFs and turbulence are investigated in ECRH plasmas using the conditional average analysis further. Figure 11(a) shows the contour plot of the conditional average of the relative intensity of potential fluctuations in the LFZF frequency bands of 0.5–3 kHz. The relative intensity is calculated as $\delta\phi_f(t)^2/\overline{\delta\phi_f(t)^2}$, where $\delta\phi_{f(t)}$ is the potential fluctuations from the radial rake probe array of 12 tips, and the overline means a time average with the same time window for each channel. The conditional average of the soft X-ray signals at the plasma center is also shown at the top of figure 11(a). At all the positions, the LFZFs decrease (increase) before (after) sawtooth crashes. The delay time of the zonal flows with respect to sawtooth crash is ~ 1 ms at the position of $r - r_L = -4.8$ cm, where r_L is the radius of the LCFS and the minus sign means from the LCFS inward. The delay time increases with the radial positions and reaches ~ 1.3 ms at $r - r_L = -0.4$ cm. The observation suggests that the LFZF propagates outward and its velocity is estimated as ~ 150 m s^{-1}. The stronger LFZFs are observed in the interval between $r - r_L = -4.8$ and -3.5 cm and between $r - r_L = -1.8$ and -0.4 cm. However, in the interval between $r - r_L = -3.5$ and -1.8 cm, the LFZF intensity becomes weaker. The contour of the intensity for the turbulence in the frequency bands of 20–200 kHz is shown in figure 11(b). The behavior of the delay time of the turbulence is similar to that of the LFZFs. The turbulence also propagates

outward and its velocity is the same as those of the LFZFs. In the interval between $r - r_L = -3.6$ and -1.8 cm, the turbulence intensity is higher where the LFZF is weaker. The results indicate that sawteeth induce not only heat-pulse propagation but also turbulence burst and flow propagation. The edge turbulence is enhanced by turbulence pulse and leads to the increase of the LFZF intensity.

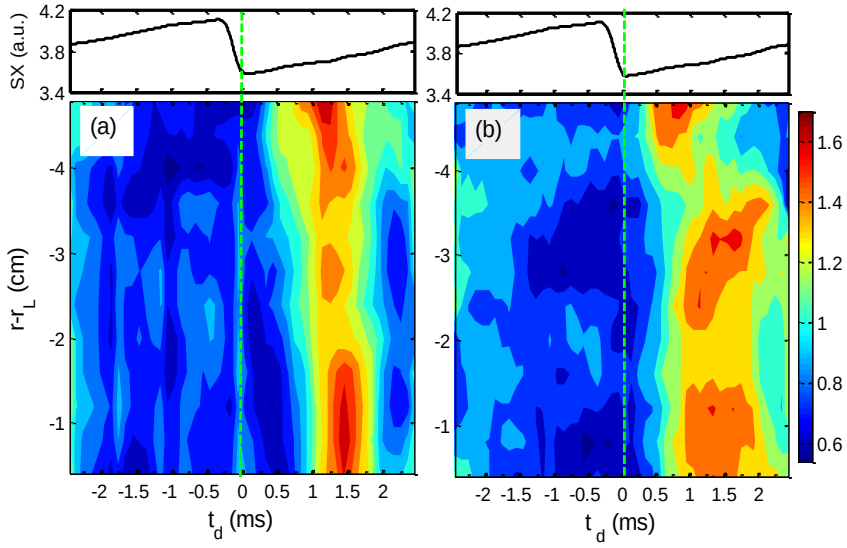

Figure 11. Conditional average of the intensities of potential fluctuations in the LFZF (a) and turbulence (b) frequency bands of 0.5–3 kHz and 20–200 kHz in various positions in L-mode plasmas with ECRH power ~ 500 kW, respectively. The conditional average of the soft X-ray signals at the plasma center is given at the top of figures (a) and (b).

3.6. Sawtooth-triggered I-phases

The characteristics of flows and turbulence in the interval between sawtooth crashes and I-phases are measured to explore the roles of turbulence and flows in sawtooth-triggered L-I transitions. The probe with two steps and 12 tips is inserted into plasmas ~ 1 cm. Figures 12(a)–(e) present the soft X-ray signals, D_α signals, E_r, electron density, and turbulence intensity in the frequency bands of 20–200 kHz in NBI plasmas, respectively. The sawtooth crash occurs at 610.3 ms. Following the sawtooth crash, the L-I transition is observed at 611.2 ms. That is the delay time of the L-I transition with respect to sawtooth crash by about 0.9 ms. After the L-I transition, the D_α, E_r, electron density, and turbulence intensities all become an oscillation. In the interval between 610.3 and 611.2 ms, a peaked turbulence intensity appears and corresponds

to a negative E_r peak. The negative peak indicates that the E_r is enhanced. The phase relation between turbulence and flows is consistent with the observation above where the flows and turbulence are nearly out of phase. There is no significant increase in density between sawtooth crashes and L-I transitions. Normally, the zonal flows are considered to suppress turbulence and reduce turbulent transport. Following sawtooth crashes, the turbulence reaches the edge and enhances the zonal flows. Inversely, the enhanced zonal flow suppresses turbulence and then the plasma jumps into the I-phase. Thus, this observation suggests sawtooth heat pulses trigger L-I transition through enhancing edge turbulence and flows.

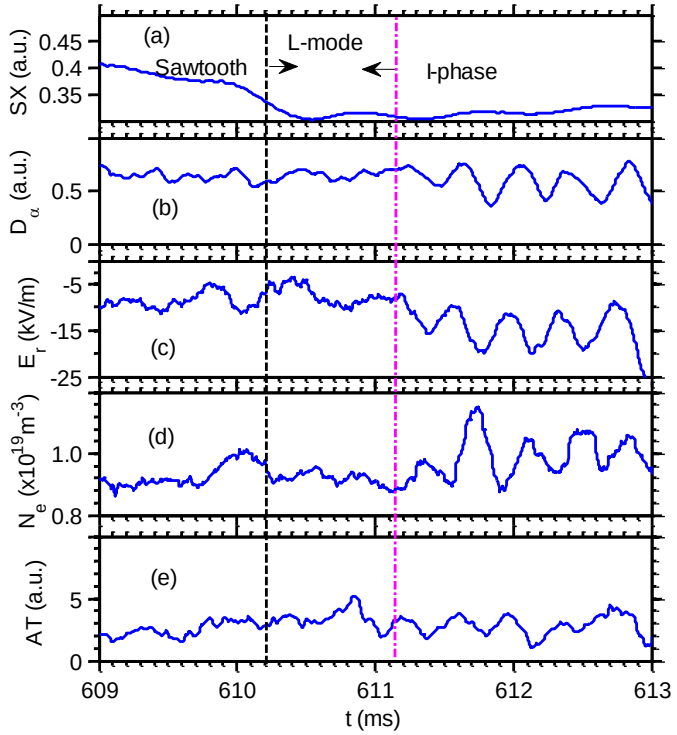

Figure 12. (a) Soft X-ray signals at plasma center, (b) D_α signals, (c) radial electric field, (d) electron density and (e) turbulence intensity in NBI plasmas.

To explore the correlation between such L-I transitions and sawtooth crashes further, the time delay of the L-I transitions with respect to sawtooth crashes is analyzed statistically. The probability density function (PDF) of the delay time for the L-I transitions, following the sawtooth crashes is given in figure 13. Over one hundred of such L-I transitions are included for this analysis. The higher value of the PDF is shown in the interval of ~ 0.3–1.2 ms and a

significant peak in the PDF appears at ~ 0.6 ms. The analysis indicates that the L-I transitions are most likely to happen at ~ 0.3–1.2 ms after sawtooth crashes, especially at ~ 0.6 ms. However, if the delay time is less than 0.2 ms or more than 1.5 ms, the L-I transition might not be caused by sawtooth crashes because of the small values of the PDF. The observation indicates that the delay time of L-I transitions with respect to sawtooth crashes is comparable to that of flows and turbulence in ECRH plasmas ~ 1 ms as above. The result also suggests that the L-I transitions can be caused by increasing flows due to sawtooth crashes.

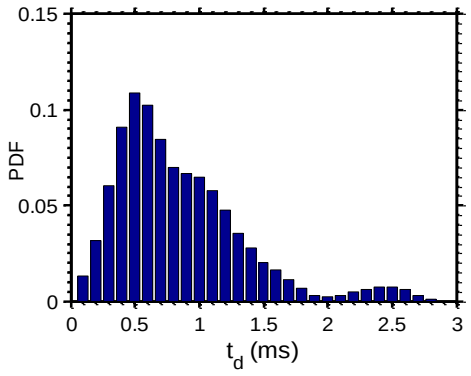

Figure 13. The probability distribution functions of the delay times for the L-I transitions, following sawtooth heat pulses in NBI plasmas.

4. Conclusion and discussion

Sawtooth heat pulse propagation is an important issue in the fusion field. However, the flow formation mechanisms during sawtooth cycles have not attracted much attention. In previous studies, sawtooth-induced density and heat-pulse propagations were mainly focused on. The heat flows and density-pulse propagation can induce temperature, density, and pressure gradient propagations. In fact, not only the density and heat pulse propagations but also turbulence clump propagation can be induced by sawteeth. Generally speaking, both gradients and turbulence contribute to flow formations. Here, the edge flows and turbulence are detected during sawtooth cycles and a double-source predator-prey model analysis is carried out. The radial electric fields, zonal flows, and turbulence are significantly enhanced due to sawteeth. The development of the turbulence is prior to the radial electric field and zonal flows. The

intensities of both the zonal flows and electric field nearly linearly increase/decrease with the increase/decrease of the turbulence intensity. The flows might be driven less effectively when the turbulence is below the critical value. The model analysis can only be part of experimental observation, just the rotation direction of hysteresis, not the other characteristics of the observation. The same rotation direction of the hystereses for the experiment observation and model calculation suggests that a relatively strong turbulence pulse is a benefit for the dominant zonal flow formation and thus L-I transitions.

The delay time of the edge electric fields, zonal flows, and turbulence with respect to the sawtooth crash is first evaluated as ~ 1 ms. Note that the importance of the delay time is embodied by the study of not only the sawtooth propagation but also the sawtooth-triggered transitions. Generally speaking, the flows are favorable for confinement regime transitions. Thus, the delay time is a key parameter to understand the underlying physics of sawtooth-induced confinement regime transitions. The fact that the estimated delay time ~ 1 ms in L-mode plasmas is comparable to that of the sawtooth - triggered L-I transitions suggests that the sawtooth heat pulses trigger L-I transitions through increasing turbulence-driven flows. Furthermore, the enhancements of the radial electric field and turbulence are observed proceeding the L-I transitions and following the sawtooth crashes.

Acknowledgments

This work is supported by National Natural Science Foundation of China (Nos. 12075057, 11775069, 11320101005 and 11875020); by National Magnetic Confinement Fusion Program of China (No. 2017YFE0301201); by East China University of Technology, Doctoral Foundation (Nos. DHBK2017134 and DHBK 2018059); by Grant-in-Aid for Scientific Research of JSPS (Nos. 15H02155, 15H02335, 16H02442); by Landmark Achievements in Nuclear Science and Technology (No. xxkjs2018011) and Natural Science Foundation of Jiangxi Province (Nos. 20202ACBL201002 and 0192ACB80006).

References

[1] von Goeler S, Stodiek W and Sauthoff N 1974 *Phys*. *Rev*. *Lett*. **33** 1201 doi:

10.1103/PhysRevLett.33.1201

[2] Wagner F *et al* 1984 *Phys*. *Rev*. *Lett*. **53** 1453 doi: 10.1103/PhysRevLett.53.1453

[3] Zhao K J *et al* 2013 *Nucl*. *Fusion* **53** 123015 doi: 10.1088/0029-5515/53/12/123015

[4] Ido T *et al* 2002 *Phys*. *Rev*. *Lett*. **88** 055006 doi: 10.1103/PhysRevLett.88.055006

[5] Martin Y R and TCV Team 2004 *Plasma Phys*. *Control*. *Fusion* **46** A77 doi: 10.1088/0741-3335/46/5A/008

[6] Nagashima Y *et al* 2016 *J*. *Phys*. *Soc*. *Jpn*. **85** 063501 doi: 10.7566/JPSJ.85.063501

[7] Chapman I T *et al* 2010 *Nucl*. *Fusion* **50** 102001 doi: 10.1088/0029-5515/50/10/102001

[8] Sauter O *et al* 2002 *Phys*. *Rev*. *Lett*. **88** 105001 doi: 10.1103/PhysRevLett.88.105001

[9] Gorini G *et al* 1993 *Phys*. *Rev*. *Lett*. **71** 2038 doi: 10.1103/PhysRevLett.71.2038

[10] Gentle K W, Austin M E and Phillips P E 2004 *Plasma Sci*. *Technol*. **6** 2130 doi: 10.1088/1009-0630/6/1/004

[11] Biglari H, Diamond P H and Terry P W 1990 *Phys*. *Fluids B* **2** 1 doi: 10.1063/1.859529

[12] Itoh S I and Itoh K 1988 *Phys*. *Rev*. *Lett*. **60** 2276 doi: 10.1103/PhysRevLett.60.2276

[13] Diamond P H *et al* 2005 *Plasma Phys*. *Control*. *Fusion* **47** R35 doi: 10.1088/0741-3335/47/5/R01

[14] Hasegawa A and Wakatani M 1987 *Phys*. *Rev*. *Lett*. **59** 1581 doi: 10.1103/PhysRevLett.59.1581

[15] Fujisawa A *et al* 2004 *Phys*. *Rev*. *Lett*. **93** 165002 doi: 10.1103/PhysRevLett.93.165002

[16] Gerrú R *et al* 2019 *Nucl*. *Fusion* **59** 106054 doi: 10.1088/1741-4326/ab34f7

[17] Pedrosa M A *et al* 2008 *Phys*. *Rev*. *Lett*. **100** 215003 doi: 10.1103/PhysRevLett.100.215003

[18] Zhao K J *et al* 2010 *Plasma Phys*. *Control*. *Fusion* **52** 124008 doi: 10.1088/0741-3335/52/12/124008

[19] Winsor N, Johnson J L and Dawson J M 1968 *Phys*. *Fluids* **11** 2448 doi: 10.1063/1.1691835

[20] Zhao K J 2006 *Phys*. *Rev*. *Lett*. **96** 255004 doi: 10.1103/PhysRevLett.96.255004

[21] Jakubowski M, Fonck R J and McKee G R 2002 *Phys*. *Rev*. *Lett*. **89** 265003 doi: 10.1103/PhysRevLett.89.265003

[22] Zhao K J *et al* 2016 *Phys*. *Rev*. *Lett*. **117** 145002 doi: 10.1103/PhysRevLett.117.145002

[23] Rhodes T L, Ritz C P and Lin H 1990 *Phys*. *Rev*. *Lett*. **65** 583 doi: 10.1103/PhysRevLett.65.583

[24] Rogister A *et al* 1986 *Nucl*. *Fusion* **26** 797 doi: 10.1088/0029-5515/26/6/008

[25] Schmitz L 2017 *Nucl*. *Fusion* **57** 025003 doi: 10.1088/1741-4326/57/2/025003

[26] Hubbard A E *et al* 2012 *Nucl*. *Fusion* **52** 114009 doi: 10.1088/0029-5515/52/11/114009

[27] Zhao K J *et al* 2015 *Nucl*. *Fusion* **55** 073022 doi: 10.1088/0029-5515/55/7/073022

[28] Zhao K J *et al* 2020 *Nucl*. *Fusion* **60** 106030 doi: 10.1088/1741-4326/abadad

[29] Zhao K J *et al* 2017 *Nucl*. *Fusion* **57** 076036 doi: 10.1088/1741-4326/aa6f35

[30] Zhao K J *et al* 2016 *Nucl*. *Fusion* **56** 076005 doi: 10.1088/0029-5515/56/7/076005

[31] Li X B, Guo Z B and Zhao K J 2020 *Plasma Phys*. *Control*. *Fusion* **62** 125018 doi: 10.1088/1361-6587/abc08c

[32] Kim E J and Diamond P H *et al* 2003 *Phys*. *Rev*. *Lett*. **90** 185006 doi: 10.1103/PhysRevLett.90.185006